The absorption indicatrix as an empirical model to describe anisotropy in X-ray absorption spectra of pyroxenes

CODY J. STEVEN^{1,2,*}, M. DARBY DYAR³, MOLLY MCCANTA^{4,†}, MATTHEW NEWVILLE⁵, AND ANTONIO LANZIROTTI^{5,‡}

¹Planetary Science Institute, Tucson, Arizona 85719-2395, U.S.A

²Department of Geological Sciences, University of Idaho, 875 Perimeter Drive, Moscow, Idaho 83843, U.S.A.

³Department of Astronomy, Mount Holyoke College, South Hadley, Massachusetts 01075, U.S.A.

⁴Department of Earth and Planetary Sciences, University of Tennessee, Knoxville, Tennessee 37996, U.S.A.

⁵Center for Advanced Radiation Sources, University of Chicago, 5640 S. Ellis Avenue, Chicago, Illinois 60637, U.S.A.

ABSTRACT

Anisotropic absorption in crystals is routinely observed in many spectroscopic methods and is recognized in visible light optics as pleochroism in crystalline materials. As with other spectroscopies, anisotropy in Fe K-edge X-ray absorption spectroscopy (XAS) can serve both as an indicator of the general structural arrangement and as a conundrum in quantifying the proportions of absorbers in crystals. In materials containing multiple absorbers, observed anisotropies can typically be represented by a linear relationship between measured spectroscopic peak intensities and relative absorber concentrations. In this study, oriented XAS analysis of pyroxenes demonstrates that the macroscopic theory that describes visible light absorption anisotropy of triaxially anisotropic materials can also be applied to X-ray absorption in pyroxenes, as long as the orientation and magnitude of the characteristic absorption vectors are known for each energy. Oriented single-crystal XAS analysis of pyroxenes also shows that the measured magnitude of characteristic absorption axes at a given orientation is energy-dependent and cannot be reproduced by linear combination of intermediate spectra. Although the macroscopic model describes a majority of the anisotropy, there is distinct discordance between the observed and interpolated spectra in the pre-edge between 7109 and 7115 eV, which is marked by spikes in RMSE/mean intensity ratio. Absorption indicatrices for samples analyzed in the visible and at X-ray wavelengths are modeled with a three-dimensional (3D) pedal surface, which functions as an empirical way of interpolating between the observed absorption data. This surface only requires a maximum of three coefficients, and results from the summation of 3D lemniscates. An absorption indicatrix model can be used to characterize anisotropic absorption in crystals and provides a way of comparing XAS spectra from randomly oriented crystals, such as those from polished sections, to a database of characterized crystals.

Keywords: Pyroxene, XANES, anisotropy, absorption, indicatrix

Introduction

X-ray absorption spectroscopy (XAS) is a highly sensitive technique for quantifying the speciation and valence state of major and trace elements in geologically relevant materials. For quantifying Fe redox ratios in minerals and magmatic glasses, Mössbauer and X-ray absorption spectroscopies are today the most sensitive techniques available and most frequently used. Fe K-edge XAS is particularly useful due to the micrometer-scale spatial resolution and detection limits of only a few parts per million. In silicate glasses, several calibrations have established the relationship between XANES spectra and Fe³⁺/ Σ Fe (Berry et al. 2003; Cottrell et al. 2009; Dyar et al. 2016b; Brounce et al. 2017). Many early investigations used the pre-edge region to predict Fe³⁺ concentration using peak centroid and area ratio (Bajt et al. 1994; Petit et al. 2001; Wilke et al. 2004) because this region represents the bound states to the 3d level in iron.

However, there are many issues with determining valence state using pre-edge features. Quantitative measures that use only the pre-edge region are bound by small-number statistics as the pre-edge is far less intense than the rest of XAS. Pre-edge peaks in crystals represent split energy levels, with absorbers often occupying multiple sites and peak energies reflecting both the amount of each species present and the geometries of the sites in which they reside. The energy of a transition is dictated by the type of cation and coordinating anions, the oxidation state of the cation, the coordination number, and the symmetry of coordinating polyhedron (Burns 1993).

Knowledge of the allowable transitions in the ligand environment of the absorber is required to assign specific absorption peaks. Given the difference in size between trivalent and divalent elements, this results in slightly higher energy transitions for trivalent species than for divalent ones. Thus, for many materials, the peak area-adjusted pre-edge centroid can provide a reasonable direct measurement of valence state (Petit et al. 2001; Wilke et al. 2004; Muñoz et al. 2013).

In anisotropic single crystals, interpretation of X-ray absorp-

^{*} E-mail: csteven@psi.edu

[†] Orcid 0000-0001-9486-8908

[‡] Orcid 0000-0002-7597-5924

tion spectra across the entire main-edge region is complicated by the inherent polarization of the X-ray beam at a synchrotron source. The resulting interactions with anisotropic crystals have the potential to obscure potentially quantitative relationships among absorptions at particular energies and valence states. This study seeks to better understand how anisotropy in pyroxenes affects the measured shape and orientation of the absorption indicatrix as a function of incident X-ray energy, building upon analogies to visible light, which has been well-studied. Presented here are the results of XAS measurements made on a series of single-crystal pyroxenes precisely oriented with respect to the incident X-ray beam using a universal stage assembly incorporated within the beamline configuration. These measurements are then used to locate the axes of absorption extremes needed to build the indicatrix. Once described, such an indicatrix can be employed to model characteristics of Fe K-edge XAS data from single pyroxene crystals at unknown orientations either by matching with a database calculated from characteristic orientations or by regression methods based on that database. This approach shows promise for side-stepping the issues involved with empirical calibrations for valence state that are based upon randomly oriented single crystals and provides a path forward for calibration of redox ratios using XAS in anisotropic mineral groups. Accurate estimates of relative Fe²⁺ and Fe³⁺ abundance in pyroxenes can potentially provide information regarding the oxygen fugacity of magmatic systems at equilibration and thus a system's differentiation history, any potential assimilation of materials on magma ascent, and degrees of metasomatism. Although relative proportions of Fe²⁺ and Fe³⁺ are often estimated in electron microprobe analysis on the basis of likely coupled substitutions in pyroxenes, most natural samples contain some tetrahedral Al and too many possible substitutions in the M-sites to make these estimates with high degrees of accuracy difficult. Therefore, direct measurement of Fe³⁺/ Σ Fe is still required to derive values of FeO and Fe₂O₃.

BACKGROUND

Early XAS studies of layered compounds by Heald and Stern (1977) described the influence of anisotropy from both a simple macroscopic theory and a more complex microscopic theory. The microscopic theory they described involved summation of spherical harmonics from a central absorbing atom to an array of neighboring atoms to calculate X-ray absorption spectra and their orientation dependence. Templeton and Templeton (1982, 1985) demonstrated anisotropy in isotropic materials that were attributed to molecular asymmetry rather than purely macroscopic anisotropy. The macroscopic theory of Heald and Stern was modeled as a $\cos^2\theta$ relationship from one absorption magnitude to another, similar to the way Malus's law describes light traveling through linear polarizers (Wódkiewicz 1995). In the case of layered compounds, absorption μ can be described by the component absorption directions when the incident photon beam's vibration path is oriented parallel with the layers μ_{\parallel} , and oriented with the vibration path perpendicular to the layers μ_{\perp} . The orientation dependence of absorption $\mu(\theta)$ can be described by the angular dependence θ of the absorption magnitude from the perpendicular to the parallel setting:

$$\mu(\theta) = \mu_{\parallel} + (\mu_{\perp} - \mu_{\parallel})\cos^2\theta,\tag{1}$$

equivalent to:

$$\mu(\theta) = \mu_{\perp} \cos^2 \theta + \mu_{\parallel} \sin^2 \theta, \tag{2}$$

which is a similar expression applied to the orientation absorbers due to the transition dipole moment in other spectroscopies (Kliger and Lewis 2012). By this relationship, the absorption anisotropy of a compound with three principal components can be modeled by an extension of pedal curves, which vary as a function of $\cos^2\theta$ in 3D, which is similar, but not equivalent, to Fresnel's elasticity surface. Absorption magnitudes μ in the resulting surface is described by:

$$\mu(\theta_x, \theta_y, \theta_z) = ||x|| *\cos^2 \theta_x + ||y|| *\cos^2 \theta_y + ||z|| *\cos^2 \theta_z, \tag{3}$$

in a directional cosine form, or:

$$\mu(\theta, \varphi) = (\|x\| \cos^2\theta + \|y\| \sin^2\theta) \sin^2\varphi + \|z\| \cos^2\varphi, \tag{4}$$

in polar form. Within the indicatrix model's basis, ||x||, ||y||, and ||z|| represent the characteristic absorption magnitudes along x, y, and z, which are orthogonal to one another. θ is the azimuth of a line projected from z to the x-y plane, and φ is the angle between the line and z. The right side of Equation 4 can be substituted as the scalar $\mu(\theta,\varphi)$ in the parametric equation of a sphere to plot the shape:

$$x = \mu(\theta, \phi) * \cos \phi \sin \theta$$

$$y = \mu(\theta, \phi) * \sin \phi \sin \theta$$

$$z = \mu(\theta, \phi) * \cos \phi$$
(5)

The pedal surface is related to lemniscate-shaped components, which represent individual absorbers as shown in a two-dimensional (2D) cross section in Figure 1. In a 2D cartesian basis, for *n* number of absorbers, each absorber contributes to the overall absorption indicatrix as follows:

$$x = \sum_{i=1}^{n} (\|x\|_{i} * \cos^{2}(\theta + \phi_{i}) + \|y\|_{i} * \sin^{2}(\theta + \phi_{i})) * \cos(\theta + \phi_{i})$$

$$y = \sum_{i=1}^{n} (\|x\|_{i} * \cos^{2}(\theta + \phi_{i}) + \|y\|_{i} * \sin^{2}(\theta + \phi_{i})) * \sin(\theta + \phi_{i})$$
(6)

where $\|x\|_i$ and $\|y\|_i$ are magnitudes of characteristic absorption along their respective axes in the lemniscate basis, θ is a variable, and φ_i denotes the orientation of each lemniscate in the cartesian basis. For the lemniscates, $\|y\|_i$ is always zero. In Figure 1, three absorbers contribute to the overall 2D absorption indicatrix where $\|x\|_1 = 0.02$, $\varphi_1 = 0^\circ$ for absorber 1; $\|x\|_2 = 0.01$, $\varphi_2 = 45^\circ$ for absorber 2; and $\|x\|_3 = 0.01$, $\varphi_3 = 135^\circ$ for absorber 3. Adding each absorber results in an absorption indicatrix with an orientation and coefficients that can be solved numerically, though the closed-form expression is not obvious. Although there are infinite solutions for how many lemniscate components comprise the absorption indicatrix given the variables of orientation and characteristic absorption, the absorption indicatrix is nonetheless related to these components.

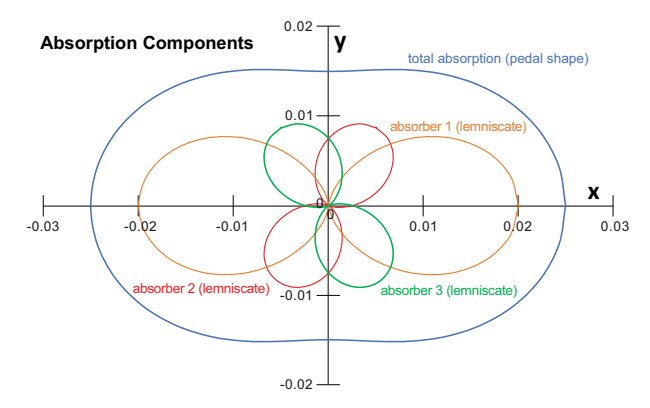


FIGURE 1. Hypothetical example of total absorption magnitude (pedal curve) decomposed into constituent absorbers (lemniscate curves) with respect to orientation in this section.

For absorption anisotropy, this surface accurately describes infrared and visible light absorption of a given wavelength in anisotropic crystals, making it useful for interpolating absorption magnitudes of intermediate orientations. The concept of an absorption indicatrix was referenced in early visible light absorption studies of minerals but was not fully understood in the mineralogy community due to the compounding effect that birefringence and the optical indicatrix have on plane-polarized light (Faye and Nickel 1970). Libowitzky and Rossman (1996) recognized this issue and brought attention to ways of navigating problems surrounding anisotropic absorption at infrared wavelengths. Similarly, in visible light optics, anisotropic absorption and vibration directions must be considered together to explain an observed absorption magnitude. What is less clear is whether the macroscopic models used to describe absorption in visible light and infrared spectroscopy effectively model the absorption behavior of X-rays in crystalline materials. In this study, X-ray absorption spectra were collected in fluorescence mode, which is the complement of absorption and is routinely used in XAS.

SAMPLES STUDIED AND METHODS

As an example of optical pleochroism, a sample of hornblende from Renfrew, Ontario, was selected for analysis from collections at the University of Idaho. Visible light absorption of amphiboles in oriented sections was measured with a Vickers spectrophotometer under interference-filtered monochromatic light (550 nm).

Pyroxenes analyzed in this study include hedenbergite HMM119666 from the Mineralogical and Geological Museum at Harvard ($Na_{0.002}Ca_{0.990}Fe_{0.34}^{2.3}$ $Mn_{0.147}Si_{1.988}$ $Al_{0.004}$ $Mg_{0.044}O_{6.000}$ and an augite megacryst, DH-218, from Dish Hill, California, collected by M.D. Dyar ($Na_{0.085}Ca_{0.756}Fe_{0.159}^{2+}Fe_{0.078}^{2+}Al_{0.136}$ $Mg_{0.740}Mn_{0.005}Si_{1.734}Al_{0.260}O_{6.00}H_{0.027}$). Unpublished archival analyses for both samples follow methods used by Dyar et al. (1989). Their composition was evaluated prior to XAS analysis by electron probe microanalysis (EPMA) and known Fe^{3+}/E^{3+} Section Mössbauer spectroscopy (unpublished work). Highly uniform crystals of hedenbergite and augite were chosen to bracket Fe^{3+} concentrations that span a common range.

Crystals were oriented initially by optical methods and crystal morphology with spindle stage techniques and the aid of the EXCELIBR program (Steven and Gunter 2017). Crystallographic orientation was verified by single-crystal X-ray diffraction and subsequent coordinate transformation of the orientation matrix to the basis of the polarized light microscope, as described in Steven and Gunter (2020). Coordinates of the crystallographic and principal optical vectors were then transformed to coincide with the orientation of a special beamline geometry. All the Fe K-edge XAS spectra were measured using the 13-ID-E undulator-based microprobe at the GeoSoilEnviro-CARS sector, Advanced Photon Source (APS), Argonne National Laboratory, U.S.A. The optical and instrumental configuration of the beamline are described in Sutton et al. (2017). Monochromatic radiation was provided by a cryogenically cooled, double-crystal monochromator using a Si(311) monochromator crystal set. Beam focusing to the sample is provided by a pair of 240 mm long, highly polished, dynamically bent bare silicon mirrors in a Kirkpatrick-Baez (KB) geometry capable of generating focused spot sizes of ~1 × 2 μ m (FWHM) and of providing incident monochromatic flux (I_0) in excess of 5×10^{12} ph/s, which is measured in a helium-filled, 200 mm long ion chamber just upstream of the KB mirror optics.

For these experiments, the incident X-ray beam is oriented orthogonal to the sample stage, and a solid-state detector sits nearly 90° offset to detect X-ray fluorescence from the sample (Fig. 2). The fluorescence spectra were collected using a Vortex ME4 silicon-drift diode detector array coupled to a high-speed digital spectrometer system (Quantum Xpress3). Incident X-ray energy was calibrated on the first derivative peak of an iron metal foil standard (7110.75 eV, Kraft et al. 1996) and no energy drift was detected throughout the analytical session. Spectra were collected with a step size of 0.1 eV from 7101 to 7141.9 eV with a count time of 1 s/step and normalized in the software Larch (Newville 2013). Specific plane orientations were obtained by manipulating arc goniometer settings optimized from rotation matrix calculations (Fig. 3). Oriented XANES spectra targeting energies

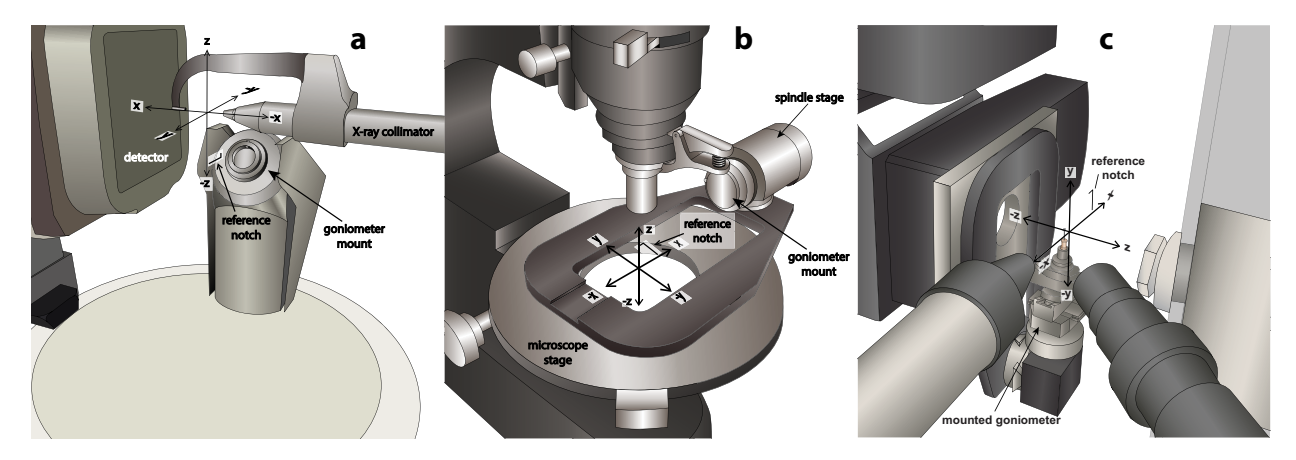


FIGURE 2. Coordinate systems used by (a) a SC-XRD, (b) a polarized light microscope as defined by EXCELIBR and EXCALIBR, and (c) the coordinate system chosen at Argonne National Laboratory. A reference notch is given to resemble how the goniometer mounts to each instrument when the angle settings are zeroed. Superimposing the reference notches affixed with the cartesian basis of each instrument gives the correct cartesian coordinate conversion. For example, from the SC-XRD in a to the beamline geometry of b the conversion is x_{XRD} becomes $-z_{beamline}$, y_{XRD} becomes $-y_{beamline}$, and z_{XRD} becomes $-x_{beamline}$.

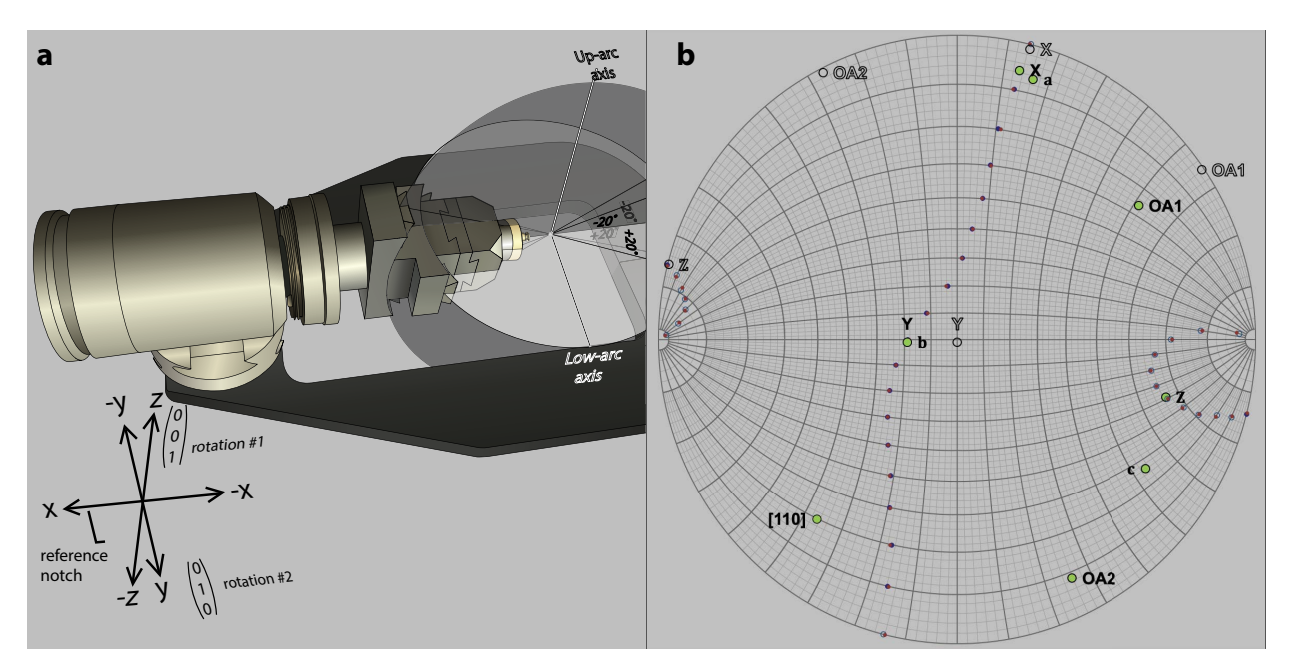


FIGURE 3. Are goniometer mounted on a spindle stage. In the zero position, the up-are axis is vertical along z, and the low-are axis is horizontal and along the y cartesian axis. Are goniometers can be used to make minor adjustments to align vectors into specific planes.

from 7108 to 7156 eV were collected on each of the two pyroxene samples in 18 orientations with the vibration path of the beam oscillating parallel with the crystal-lographic axes, which are the principal optical vectors for white light. Incremental scans were made with the beam vibrating in the (010) plane of clinopyroxenes covering a sweep of 180° (Fig. 4).

RESULTS

Visible light absorption

To demonstrate a visual example of anisotropic absorption and the effects of polarization, this section will examine the absorption indicatrix of an amphibole, edenite (Na $_{0.67}K_{0.29}$) (Ca $_{1.59}Na_{0.23}Fe_{0.13}Mn_{0.05}$)(Mg $_{2.70}Fe_{2.12}^{2+}Al_{0.15}Ti_{0.03}$)(Si $_{7.07}Al_{0.93}$) O $_{22}$ (OH) $_2$, in the visible spectrum and how it can be described

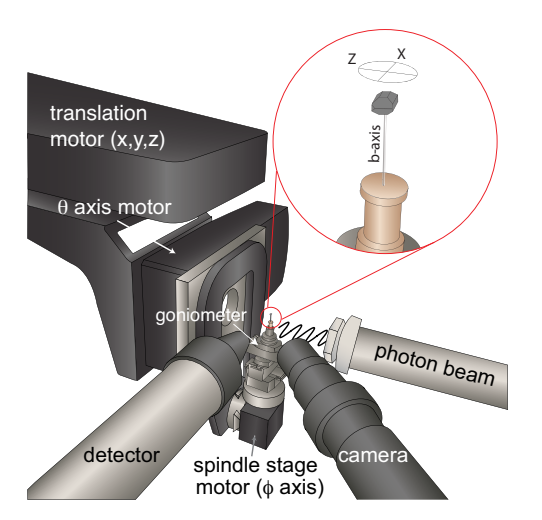


FIGURE 4. Experimental setup of a sweep scan of spectra across the plane normal to the **b** axis.

in relation to the absorption indicatrix of a mineral. An amphibole is used as a visible light analog for anisotropic absorption phenomena because pyroxenes are only weakly pleochroic. Absorption and polarization effects in amphiboles have been studied by several authors, most comprehensively by Bancroft and Burns (1969) and subsequently by Faye and Nickel (1970), who attribute absorption to charge transfer between Fe²⁺ and Fe³⁺ as well as between Fe³⁺ and O²⁻. The Fe charge transfer results in visible absorption bands centered at approximately 435, 526, and 649 nm that are significantly influenced by polarization. Faye and Nickel (1970) suggested that in some amphiboles, the absorption indicatrix and optical indicatrix apparently do not coincide.

Here, the absorption indicatrix is presented in 2D radial sections, constructed as a 3D absorption indicatrix that has the same topology as a pedal surface. If individual absorbers are responsible for the Equation 4 relationship between the orientation of the dipole transition moment and incident linear polarization direction (\vec{E}) , then multiple absorbers will always result in an absorption indicatrix with the shape of the pedal surface, which is then subject to polarization and interference effects. The area of this surface can then be used to construct a sphere of equivalent area for which the length of the radius represents the unpolarized absorption magnitude at a given wavelength. This can then be related to concentrations of absorbers after the recommendations of Libowitzky and Rossman (1996).

Fe-bearing calcic amphiboles generally have a large angle between the ${\bf c}$ axis and the principal optical vector. In this example, ${\bf c} \wedge Z$ is 30°, which is adequate for demonstrating how absorption is influenced by polarization and orientation of absorbers. The amphibole is depicted with white light and on a spindle stage, while the quantitative measurements of absorbance are described in the thin section.

The two factors contributing to the anisotropic absorption of

visible light are (1) orientations of the transition dipole moments of absorbers and (2) the orientation of \vec{E} relative to the principal vibration directions of the crystal.

A roughly cylindrical amphibole grain mounted with its c axis (along the length of the particle) parallel to the spindle stage rotation axis gives a representation of absorption magnitude that is minimally biased by differences in thickness. When aligned with \vec{E} , each principal optical vector has an associated absorption magnitude. These are not necessarily the characteristic axes of the absorption indicatrix, but are projections of absorbers onto the principal optical vectors (Libowitzky and Rossman 1996). Absorption observed along any vibration direction is unaffected by anisotropy due to interference but is influenced by anisotropy due to absorber orientations. The Z optical vector is orthogonal to the Y = **b** axis at an angle of 30° to the **c** axis. Because the c axis of a typical hornblende grain is not a principal vibration direction, orienting the c axis parallel to the \vec{E} will result in different absorption values as the spindle axis is rotated, despite being cylindrical. Rotating the spindle axis until the grain is at extinction in cross-polarized light indicates an orientation in which E remains linearly polarized and East-West through the crystal. This vibration direction is a Z' direction, which is 90° to the Y optical vector in the plane of the stage. The absorption along the c axis in this orientation gives the true absorbance of the c axis rather than an intermediate absorbance that depends on the angle from the vibration directions.

In interfering positions, visible light is considered to be vibrating along two vibration directions that are not coincident with the initial \vec{E} . This results in an absorption magnitude that is intermediate to those observed along the vibration directions in that section (Fig. 5b). For example, there is more absorption when \vec{E} is parallel to the $\bf c$ axis if it is a vibration direction (Fig. 5e) than when the $\bf c$ axis is parallel to the initial \vec{E} but not a vibration direction (Fig. 5b). When \vec{E} is parallel to $\bf Y = \bf b$ axis, the crystal

absorbs the most light due to the orientation and distribution of charge-transfer absorbers (Faye and Nickel 1970).

Based on the observations by Faye and Nickel (1970) and from the spindle stage example, polished sections of (100) and normal to the **c** axis were prepared to measure absorbance with 550 nm light along the characteristic axes of the absorption indicatrix. Polished sections of (100) and parallel to **c** ensure that the characteristic axes (the **c**, **b**, and normal to **c** and **b**) are in the section. This allows absorption along the **b** axis to be measured twice so the data sets can be scaled to one another. The resulting indicatrix and its orientation relative to the crystallographic orientation are depicted in Figure 6.

X-ray absorption

XAS from the two pyroxenes were collected along the crystallographic axes and various axes orthogonal to the **b** axis to explore the range of absorption magnitudes as a function of pyroxene group and composition. Both crystallographic vectors **a**, **b**, **c**, and principal optical vectors for visible light X, Y, and Z were used as reference lines for keeping track of orientation. Detailed scans with the X-ray beam vibrating along the **b** axis and in increments within the (010) plane reveal the observed range of absorption magnitude with respect to orientation and energy (Fig. 7). Radial plots from 7108.0 to 7156.0 eV are included in the Online Materials¹ as videos.

DH-218

Out of all analyzed orientations, there are four distinct preedge peaks centered at 7111.0, 7111.9, 7112.7, and 7114.1 eV in DH-218 (Fig. 7). Just below the rising edge is a peak centered at about 7117.5 eV, which is most intense when \vec{E} is parallel to the **b** axis, and the rising edge has three inflection points at 7121.2, 7123.4, and 7125.8 eV. Pre-edge peaks for octahedrally coordinated transition metal oxides correspond to quadrupole

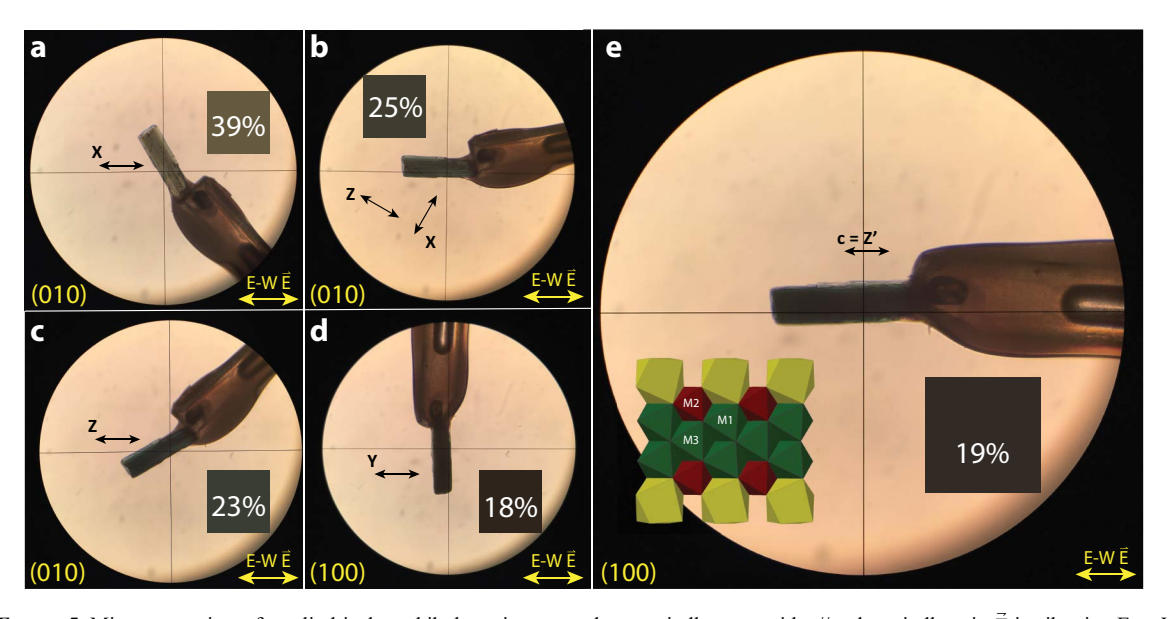


FIGURE 5. Microscope view of a cylindrical amphibole grain mounted on a spindle stage with **c**//to the spindle axis. \tilde{E} is vibrating East-West and (**a**) parallel to the X optical vector (**b**) the crystal is in an interfering position where the polarization state of light is split among X and Z (**c**) parallel to Z (**d**) parallel to Y and (**e**) parallel to a Z' vibration direction.

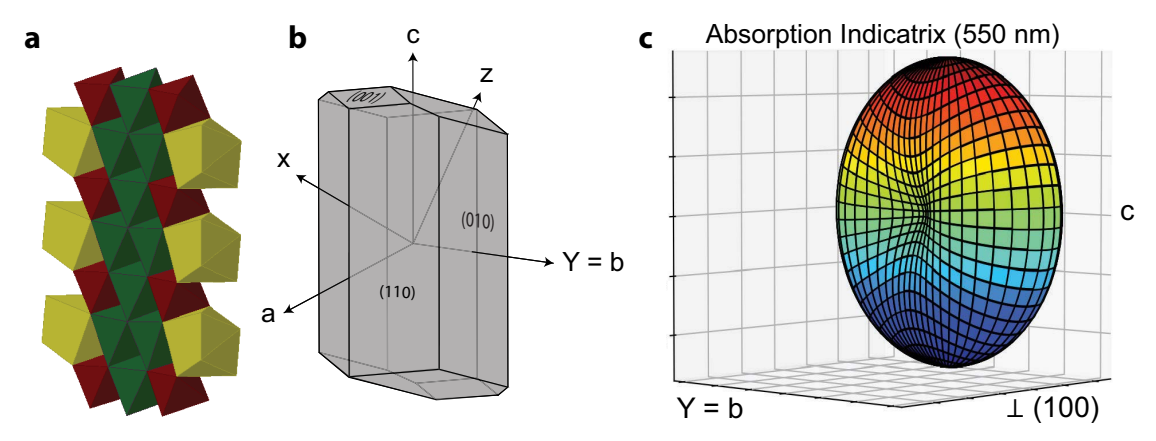


FIGURE 6. Perspective figures in like-orientations of an amphibole showing (a) the distribution of M-sites in the crystal structure (b) the crystallographic and optical vectors (c) the absorption indicatrix observed with 550 nm light.

transitions from the 1s to 3d level (De Groot et al. 2009). A similar feature to the 7117.5 eV peak has been described in XANES spectra of Cu oxide coordinating complexes, where charge transfer between Cu and O is believed to lower the final energy state of the 1s to $4p_z$ transition (Choy et al. 1994; Furnare et al. 2005). The rising edge of DH-218 is strongly influenced by orientation, and this sample contains mixed Fe²⁺ and Fe³⁺, but the edge itself corresponds to 1s to 4p dipole transitions of Fe²⁺ and Fe³⁺ (De Groot et al. 2009).

Radial plots of absorption magnitude geometry for DH-218 show that observed magnitudes at all energies are accurately modeled with the absorption indicatrix from energies beginning near the tail of the 4p transition (~7119 eV) and above by an ordinary least-squares fit of the pedal surface to the observed intensity data (Fig. 8). In the pre-edge, the 3d transitions are notably discordant from the macroscopic model, as indicated by the high ratio of the model root mean square error (RMSE) divided by the mean intensity ratio at the lowest energies (Fig. 9).

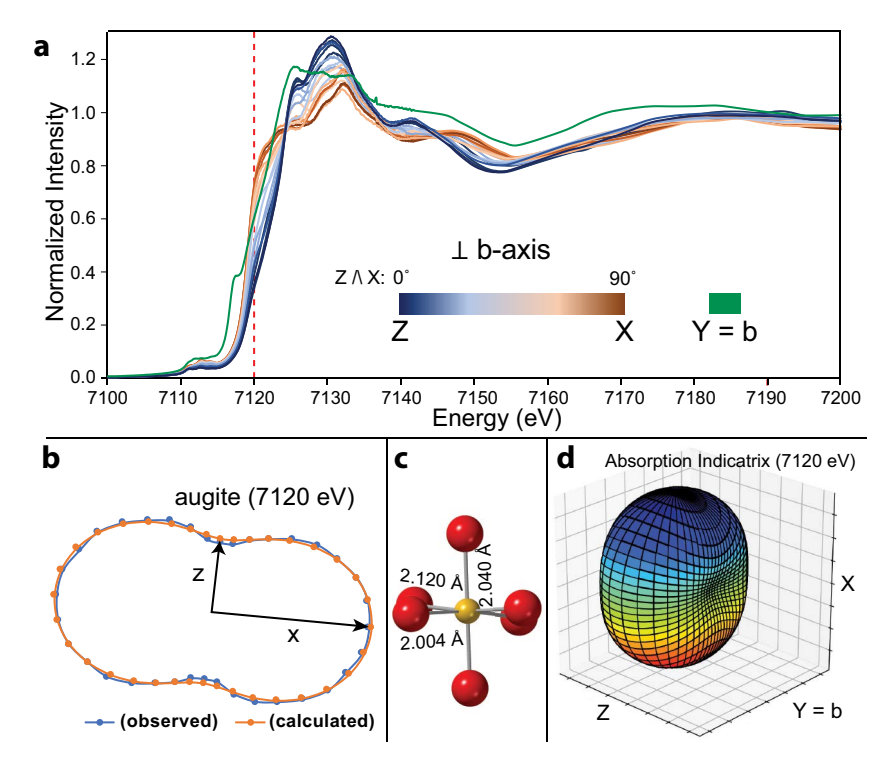


FIGURE 7. (a) Results of X-ray absorption spectra collected with \vec{E} parallel to Y = **b** and in increments of 10° with \vec{E} parallel (010) for DH-218; (b) radial plot at 7120 eV of absorption magnitude in the (010) plane relative to an octahedron of FeO; and (c) three-dimensional plot of the absorption indicatrix at 7120 eV. The orientation of absorption magnitude from **b** and the orientation of the Fe octahedron from **c** are depicted in coincidence. The vertical 2.040 Å bond is in the plane of view, and approximately corresponds with the lower absorption magnitude from **b**. The 2.004 and 2.120 Å bonds are 45° from the plane of view in **b**.

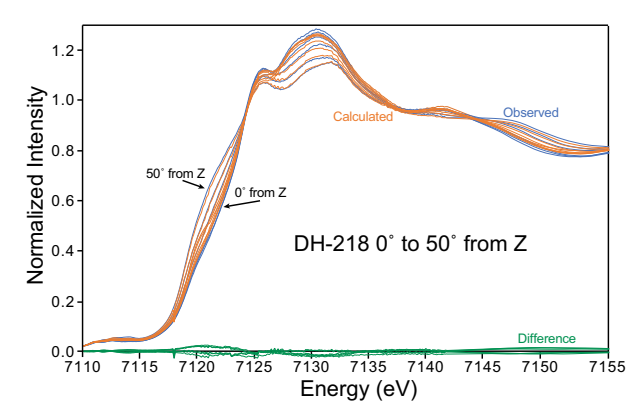


FIGURE 8. Observed and calculated spectra spanning from 0 to 50° from the Z optical vector. The discrepancy is given in green.

Orientations of minimum and maximum absorption vary as a function of energy. Plotting all orientations across (010), the absorption intensities for the rising edge energies of DH-218 are weakest when \vec{E} is along the line of the bonds and strongest when aligned in the direction of the $e_{\rm g}$ lobes.

HMM119666

HMM119666 is a purely Fe²⁺ clinopyroxene with pre-edge peaks centered at 7110.9, 7111.8, and 7113.1 eV. In contrast with DH-218, the rising edge of HMM119666 has a single inflection for the rising edge at 7120.4 eV with no additional shoulders, even among the various orientations. In both HMM119666 and DH-218, the energy just above the rising edge has isotropic absorption (Fig. 9). This has also been the case for other pyroxenes scanned along the optical and crystallographic vectors X, $Y = \mathbf{b}$, Z, \mathbf{a} , and \mathbf{c} .

DISCUSSION

Efficacy of the absorption indicatrix model at X-ray wavelengths

Scans with the vibration path in the (010) plane show that the absorption magnitudes for X-ray wavelengths are still approximated with Equation 4 (Fig. 7b). Although a full hemisphere of scans has not been collected, scans along the **b** axis and in the (010) plane cover a wide range of absorption magnitudes if not all based on symmetry. In lower energy spectroscopies such as UV-Vis, the transition dipole moment of an absorber at a given wavelength is projected along the principal polarization directions, which gives rise to the shape of absorption indicatrix. Both individual absorbers and degenerate absorbers create an indicatrix that can be modeled by the shape of the pedal surface. In the UV-Vis, if a single absorber is targeted with linearly polarized light, then two of the characteristic absorption coefficients are zero and the third is nonzero in Equation 4.

The pre-edge region comprises the least intense peaks in a XANES spectrum, which are attributed to the 3*d* transitions of Fe. Pre-edge peaks are most susceptible to discordance from the macroscopic model due to data processing errors arising from the normalization procedure. As shown in the Online Materials¹, HMM119666 has an erratic absorption geometry in the pre-edge.

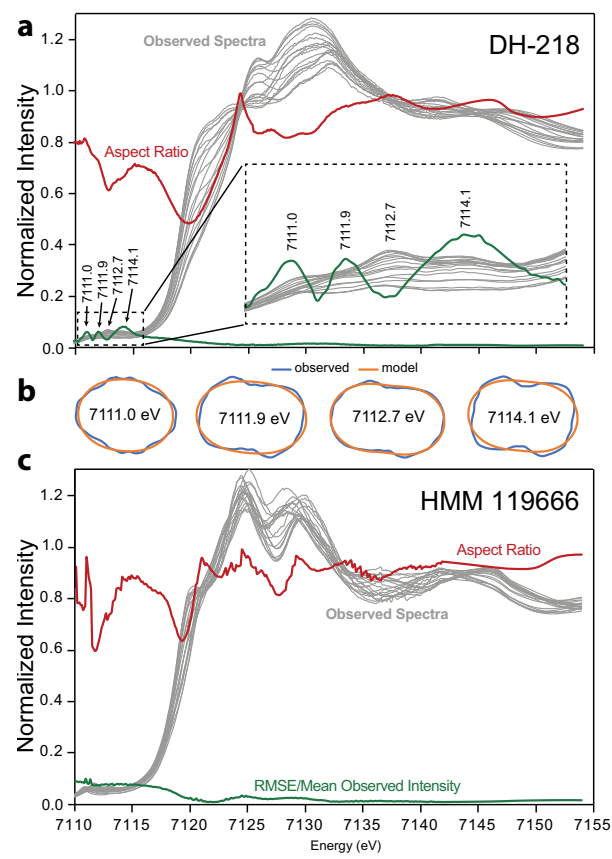


FIGURE 9. (a) Observed spectra, aspect ratio of the characteristic absorption axes, and RMSE/mean observed intensity of DH-218 (b) 2D absorption anisotropy of the pre-edge peaks in the (010) section of DH-218 at 7111.0, 7111.9, 7112.7, and 7114.1 eV. (c) Observed spectra, aspect ratio of the characteristic absorption axes, and RMSE/mean observed intensity of HMM119666. RMSE is based on the discrepancy between the observed absorption data and the macroscopic model after an ordinary least-square fit.

This can, in part, be attributed to data processing error because this scan is hedenbergite with an M1 site fully occupied by Fe²⁺, making it subject to the most discrepancy from overabsorption and dead time correction error. However, these spikes may be real byproducts of the coordinating environment of Fe, such as local geometry or charge transfer effects, which would be accentuated in samples with large amounts of Fe. Despite the error, it is small relative to the scale of the overall spectrum and is only significant in the pre-edge in terms of scale.

Data for sample DH-218 were much easier to place on the same scale in spite of the anisotropy, and the model discrepancy in those pre-edge spectra is likely demonstrating real differences in the nature of the anisotropy as shown in the Online Materials¹. Improved pre-edge data will be required to judge the geometry of the absorption anisotropy. The peak at 7117.5 eV only occurs in clinopyroxenes of mixed Fe²⁺ and Fe³⁺ and is only apparent when \vec{E} is parallel to the **b** axis. Based on these two characteristics, this peak may arise as a result of lowering the 1 s to 4p transition energy due to metal-to-metal intervalence charge transfer if Fe²⁺ largely occupies M1, while Fe³⁺ occupies M2 or M2'.

The observed differences between model and measured pre-edge data may be related to the fact that the pre-edge peaks represent absorption from quadrupole transitions rather than dipole transitions. Because the pre-edge encompasses quadrupole transitions to the 3d states from the initial 1s state at the K-edge, there are multiple absorbers that contribute to the absorption indicatrix at X-ray wavelengths. Even in that case, the shape of the indicatrix should be the same because it is comprised of absorbers that vary in absorption magnitude as a function of Equation 4 (Fig. 7b). The orientation of the principal axes of absorption indicatrix is not immediately obvious because there may be multiple absorbers of the same energy-oriented with transition dipole moments extending from an absorbing atom in 3D. It is unclear if X-ray absorption spectra are influenced by macroscopic polarization through the crystal, as with UV-VIS and infrared spectroscopy. In those cases with random sections of anisotropic crystals, the effects of absorbers are projected onto the vibration directions of light, which also form a similar absorption indicatrix. However, the absorption indicatrix depends on the section through which light is propagating in the crystal because the vibration directions depend on the orientation of the optical indicatrix. Regardless of the number of absorbers and polarization effects, the absorption indicatrix is an empirical way of describing absorption in three dimensions. The largest discrepancies from the Equation 4 model are with the 7111.0, 7111.9, and 7114.1 eV pre-edge peaks, whereas the 7112.7 eV peak is reasonably accounted for (Fig. 9). The remainder of the spectrum from the rising edge is also effectively accounted for by Equation 4. Perhaps the most mysterious aspect of the absorption magnitudes of the pre-edge and a rising edge is that the absorption magnitude is consistently largest when É is applied parallel to the lobes of the t_{2g} orbitals rather than the e_g orbitals (Fig. 7).

Application of the absorption indicatrix

Understanding the orientation and magnitudes of absorption allows spectra to be related to concentrations. For example, the volume of the absorption indicatrix can be used for comparison among anisotropic materials, similar to the unpolarizing approach used by Libowitzky and Rossman (1996). Alternatively, XAS of known random orientations can be compared to a database containing known absorption indicatrices across a range of energies by selecting the data set with the smallest residuals between the interpolated and observed spectra.

Specifically, this is done by recording the coordinates of the incident photon's vibration direction \vec{E} indexed relative to the pyroxene's crystallographic basis. Describing the coordinates relative to the crystallographic basis standardizes the orientation in which a spectrum is collected. Those coordinates are then transformed to the absorption indicatrix basis of each database pyroxene at each energy. This is done because the indicatrix orientation and absorption magnitudes vary depending on energy and composition relative to the crystallographic basis, and using the orthogonal basis of the absorption indicatrix allows absorption magnitudes of the unknown pyroxene, $\mu(\theta_x,\theta_y,\theta_z)$, to be calculated with Equation 3. The angles between \vec{E} and the absorption indicatrix basis vectors are used to solve Equation 3 so that the calculated intensity can be compared to the database intensity for the orientation of \vec{E} at each energy. Consider a scan

is collected with \vec{E} along (-0.2211, 0, 0.9752) with respect to the crystallographic basis of DH-218. Compared with the correct database composition, in this case itself, the scan intensities $\mu(\theta_{\nu},\theta_{\nu},\theta_{z})$ have an overall discrepancy

$$\frac{\sum \left\|I_{\mathrm{obs}}\right| - \left|I_{\mathrm{calc}}\right\|}{\sum \left|I_{\mathrm{obs}}\right|}$$

of 0.012 for the range from 7108.1 to 7141.8 eV and step size of 0.1 eV. This minor discrepancy suggests that the unknown DH-218 (0.33 Fe³⁺/ Σ Fe) does, in fact, match the composition of the database DH-218. The only reason the discrepancy is nonzero in this example is due to the difference between the indicatrix model and observed absorption magnitudes. However, if the unknown was HMM119666 (0.00 Fe³⁺/ Σ Fe), the discrepancy of a spectrum collected in the same orientation has a relatively large discrepancy of 0.186 from the indicatrix model of the DH-218 composition. Therefore, it does not correspond with the Fe³⁺/ Σ Fe of DH-218. Given a larger database of anisotropy models of pyroxenes with known Fe³⁺/ Σ Fe, spectra of known random orientations can be matched.

Each composition of pyroxene will have differences in absorption anisotropy and varying amounts of Fe³⁺ and Fe²⁺. The variations of orientation and relative magnitudes of the absorption indicatrix make X-ray absorption spectra of monoclinic and triclinic crystals complicated but also add to the uniqueness of each composition, making them easier to match to a database. We plan to construct a database of absorption indicatrices of end-member and intermediate orientations (the latter derived from modeling the former) across the XAS region of pyroxenes with known Fe³⁺ and Fe²⁺ concentration, such that any randomly oriented spectrum in the XAS region can be matched to it to measure redox state. This technique will be successful if each specific composition is distinctive enough to be used to match unknowns. Knowledge of the orientation of the unknown crystal would improve the accuracy of this matching technique but may not necessarily be required, depending on the overlaps in spectral features.

The symmetry of the absorption indicatrix allows polar angles and principal absorption magnitudes to be used to interpolate absorption of any given orientation. For UV-Vis and infrared spectroscopy, X, Y, and Z are fixed for orthorhombic crystals. In monoclinic crystals, the component that represents the **b** axis is fixed and the other two components are variable depending on wavelength, and in triclinic minerals all are potentially variable. The importance of this anisotropy relationship is a common value of total absorbance can be related to reflect contributions due to Fe²⁺ and Fe³⁺ within an unpolarized spectra. The procedure for calculating an unpolarized spectra is described in Libowitzky and Rossman (1996) as applied to infrared spectroscopy.

Although infrared wavelengths and X-ray wavelengths are worlds apart, some of the same concepts can be applied to the absorption indicatrix for quantifying concentrations in both energy ranges. Total absorbance for any anisotropic crystal in the visible spectrum can be determined with either universal stage, or spindle stage techniques using the polarization directions. At X-ray wavelengths, the orientations of the characteristic absorption axes at each energy are unknown but will depend on

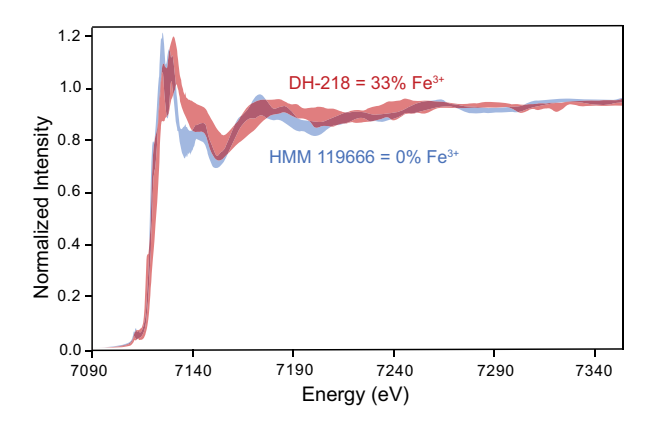


FIGURE 10. The range of absorption magnitudes of DH-218 and HMM119666 superimposed.

the dipole or quadrupole moment of electronic transitions for the near edge features. The coordination number along with the degeneracy of coordinating oxygen also contribute significantly to the pre-edge features (Wilke et al. 2001). Random unknown orientations may also be matched, but only to ranges of absorption magnitude, where several pyroxene compositions will overlap across various energy ranges (Fig. 10).

As needed, orientation can be determined either from electron backscatter diffraction (EBSD) or from universal stage methods. With Universal Stage methods, optical vectors and cleavage planes may be used in conjunction with reference texts to determine orientation of crystals in thin section Philips (1971). A refined optical orientation may also be obtained with extinction curve methods, originally discussed by Joel and Muir (1958). A similar procedure follows with EBSD orientation solution but with the appropriate coordinate transformation from the EBSD setup.

IMPLICATIONS

Equation 4 describes the general absorption anisotropy of each composition well. However, the fine details of the pre-edge have conspicuous discordances from this model. This may be due to contributions from quadrupolar electronic transitions. Our group is currently constructing a database of pyroxene spectra from samples oriented along various orientations for the purpose of understanding and navigating anisotropy issues for quantifying $Fe^{3+}/\Sigma Fe$.

Although the current database can directly predict Fe³⁺ and Fe²⁺ from specific orientations of crystals, the method can be extended to analyzing crystals in polished sections because the indicatrix model is reasonably effective. We have not yet designed a database that contains the intermediate modeled spectra for handling random orientations of crystals in the polished section. Using relationships between absorption geometry and crystallographic orientation, we plan to investigate features in XANES spectra of mixed Fe²⁺ and Fe³⁺. This paves the way for polished sections of individual crystals to be probed for Fe³⁺ content with high spatial resolution, giving indications of redox histories of crystals and Fe³⁺ content when sample volume is restricted.

The application for polished sections is based on the typical sample geometry of an XAS experiment (45° incidence and collection angles) and restrictions of stage rotation mounted 45° to the X-ray source. Spectra collected along orientations that are 90° apart in this geometry lend more information about the absorption magnitudes of the unknown. This is a sufficient range to match a set of spectra to a database pyroxene by applying the geometric constraints of the absorption indicatrix to a matching program. Such an approach to anisotropy better allows for the full XAS spectral range to be used for determining Fe³⁺ content and should represent a significant improvement over methods that rely on the low-intensity absorption data of the pre-edge alone. Absorption anisotropy in the pre-edge still needs further investigation to determine if there is a simple model for describing it. Calibrations that utilize the pre-edge can greatly benefit from an understanding of the absorption anisotropy in this region and are demonstrated here to have the most discrepancy with the absorption indicatrix model.

ACKNOWLEDGMENTS AND FUNDING

We thank Cai Ytsma for assistance with data processing, and two anonymous reviewers for insight that greatly improved this manuscript. We are grateful for support from NASA grant 80NSSC19K1008 (M.C.M.) and NSF grants EAR-1754261 (M.D.D.) and EAR-1754268 (M.C.M.).

REFERENCES CITED

Bajt, S., Sutton, S.R., and Delaney, J.S. (1994) X-ray microprobe analysis of iron oxidation states in silicates and oxides using X-ray absorption near edge structure (XANES). Geochimica et Cosmochimica Acta, 58, 5209–5214.

Bancroft, G.M., and Burns, R.G. (1969) Correlations of Mossbauer and infrared spectral data in site population studies in amphiboles. In J.J. Papike, Ed., Mineralogical Society of America Special Paper Number Two: Pyroxenes and Amphiboles: Crystal Chemistry and Phase Petrology, p. 137–148. http:// www.minsocam.org/msa/Special_Papers/#SP2

Berry, A.J., O'Neill, H.St.C., Jayasuriya, K.D., Campbell, S.J., and Foran, G.J. (2003) XANES calibrations for the oxidation state of iron in a silicate glass. American Mineralogist, 88, 967–977.

Brounce, M., Stolper, E., and Eiler, J. (2017) Redox variations in Mauna Kea lavas, the oxygen fugacity of the Hawaiian plume, and the role of volcanic gases in Earth's oxygenation. Proceedings of the National Academy of Sciences, 114, 8997–9002.

Burns, R.G. (1993) Mineralogical Applications of Crystal Field Theory, vol. 5. Cambridge University Press.

Choy, J.H., Kim, D.K., Hwang, S.H., and Demazeau, G. (1994) Cu K-edge X-rayabsorption spectroscopic study on the octahedrally coordinated trivalent copper in the perovskite-related compounds La₂Li_{0.2}Cu_{0.3}O₄ and LaCuO₃. Physical Review B, Condensed Matter, 50, 16631–16639.

Cottrell, E., Kelley, K.A., Lanzirotti, A., and Fischer, R.A. (2009) High-precision determination of iron oxidation state in silicate glasses using XANES. Chemical Geology, 268, 167–179.

De Groot, F., Vankó, G., and Glatzel, P. (2009) The 1s X-ray absorption pre-edge structures in transition metal oxides. Journal of Physics, Condensed Matter, 21, 104207.

Dyar, M.D., McGuire, A.V., and Ziegler, R.D. (1989) Redox equilibria and crystal chemistry of coexisting minerals from spinel lherzolite mantle xenoliths. American Mineralogist, 74, 969–980.

Dyar, M.D., Breves, E.A., Gunter, M.E., Lanzirotti, A., Tucker, J.M., Carey, C.J., Peel, S.E., Brown, E.B., Oberti, R., Lerotic, M., and Delaney, J.S. (2016a) Use of multivariate analysis for synchrotron micro-XANES analysis of iron valence state in amphiboles. American Mineralogist, 101, 1171–1189.

Dyar, M.D., McCanta, M., Breves, E., Carey, C.J., and Lanzirotti, A. (2016b) Accurate predictions of iron redox state in silicate glasses: A multivariate approach using X-ray absorption spectroscopy. American Mineralogist, 101, 744–747.

Faye, G.H., and Nickel, E.H. (1970) The effect of charge-transfer processes on the colour and pleochroism of amphiboles. The Canadian Mineralogist, 10, 616–635.

Furnare, L.J., Vailionis, A., and Strawn, D.G. (2005) Polarized XANES and EX-AFS spectroscopic investigation into copper (II) complexes on vermiculite. Geochimica et Cosmochimica Acta, 69, 5219–5231.

Heald, S.M., and Stern, E.A. (1977) Anisotropic X-ray absorption in layered compounds. Physical Review B, 16, 5549–5559.

Joel, N., and Muir, I.D. (1958) New techniques for the universal stage. I. An extinction curve method for the determination of the optical indicatrix. Mineralogical Magazine, 31, 860–877.

- Kliger, D.S., and Lewis, J.W. (2012) Polarized Light in Optics and Spectroscopy. Elsevier.
- Kraft, S., Stümpel, J., Becker, P., and Kuetgens, U. (1996) High resolution X-ray absorption spectroscopy with absolute energy calibration for the determination of absorption edge energies. Review of Scientific Instruments, 67, 681–687.
- Libowitzky, E., and Rossman, G.R. (1996) Principles of quantitative absorbance measurements in anisotropic crystals. Physics and Chemistry of Minerals, 23, 319–327.
- Muñoz, M., Vidal, O., Marcaillou, C., Pascarelli, S., Mathon, O., and Farges, F. (2013) Iron oxidation state in phyllosilicate single crystals using Fe-K pre-edge and XANES spectroscopy: Effects of the linear polarization of the synchrotron X-ray beam. American Mineralogist, 98, 1187–1197.
- Newville, M. (2013) Larch: An analysis package for XAFS and related spectroscopies. In Journal of Physics: Conference Series, 430, 012007. IOP Publishing.
- Petit, P.E., Farges, F., Wilke, M., and Solé, V.A. (2001) Determination of the iron oxidation state in Earth materials using XANES pre-edge information. Journal of Synchrotron Radiation, 8, 952–954.
- Philips, W.R. (1971) Mineral Optics: Principles and Techniques. W.H. Freeman. Steven, C.J., and Gunter, M.E. (2017) EXCELIBR: An Excel Spreadsheet for Solving the Optical Orientation of Uniaxial and Biaxial Crystals. The Microscope, 65, 147–152.
- ———(2020) EXCALIBR to EXCELIBR and the optical orientation of minerals: Correcting the optical orientation of clinoamphiboles. American Mineralogist, 105, 955–962.
- Sutton, S.R., Lanzirotti, A., Newville, M., Rivers, M.L., Eng, P., and Lefticariu, L. (2017) Spatially resolved elemental analysis, spectroscopy and diffraction at the GSECARS Sector at the Advanced Photon Source. Journal of Environmental

- Quality, 46, 1158-1165.
- Templeton, D.H., and Templeton, L.K. (1982) X-ray dichroism and polarized anomalous scattering of the uranyl ion. Acta Crystallographica Section A, 38, 62-67.
- ———(1985) X-ray dichroism and anomalous scattering of potassium tetrachloroplatinate (II). Acta Crystallographica Section A: Foundations of Crystallography, 41, 365–371.
- Wilke, M., Farges, F., Petit, P.E., Brown, G.E. Jr. and Martin, F. (2001) Oxidation state and coordination of Fe in minerals: An Fe K-XANES spectroscopic study. American Mineralogist, 86, 714–730.
- Wilke, M., Partzsch, G.M., Bernhardt, R., and Lattard, D. (2004) Determination of the iron oxidation state in basaltic glasses using XANES at the K-edge. Chemical Geology, 213, 71–87.
- Wódkiewicz, K. (1995) Classical and quantum Malus laws. Physical Review A, Atomic, Molecular, and Optical Physics, 51, 2785–2788.

Manuscript received January 1, 2021 Manuscript accepted March 24, 2021 Manuscript handled by Sasa Bajt

Endnote:

¹Deposit item AM-22-47950, Online Materials. Deposit items are free to all readers and found on the MSA website, via the specific issue's Table of Contents (go to http://www.minsocam.org/MSA/AmMin/TOC/2022/Apr2022_data/Apr2022_data.html).